Reflection-enhanced gain in traveling-wave parametric amplifiers

Reflection-enhanced gain in traveling-wave parametric amplifiers

S. Kern [1,*] P. Neilinger [1,2] E. Il'ichev [3] A. Sultanov [4] M. Schmelz [3] S. Linzen [3] J. Kunert,[3] G. Oelsner [3] R. Stolz,[3] A. Danilov,[5] S. Mahashabde [5] A. Jayaraman [5] V. Antonov [6] S. Kubatkin [5] and M. Grajcar [1,2]

[1]*Department of Experimental Physics, Comenius University, SK-84248 Bratislava, Slovakia*
[2]*Institute of Physics, Slovak Academy of Sciences, Dúbravská cesta, SK-84228 Bratislava, Slovakia*
[3]*Leibniz Institute of Photonic Technology, D-07702 Jena, Germany*
[4]*Department of Applied Physics, Aalto University, P.O. Box 15100, FI-00076 Aalto, Finland*
[5]*Department of Microtechnology and Nanoscience MC2, Chalmers University of Technology, SE-41296 Goteborg, Sweden*
[6]*Physics Department, Royal Holloway, University of London, Egham TW20 0EX, United Kingdom*

(Received 8 March 2022; revised 4 May 2023; accepted 8 May 2023; published 22 May 2023)

The operating principle of traveling-wave parametric amplifiers is typically understood in terms of the standard coupled mode theory, which describes the evolution of forward propagating waves without any reflections, i.e., for perfect impedance matching. However, in practice, superconducting microwave amplifiers are unmatched nonlinear finite-length devices, where the reflecting waves undergo complex parametric processes, not described by the standard coupled mode theory. Here, we present an analytical solution for the TWPA gain, which includes the interaction of reflected waves. These reflections result in corrections to the well-known results of the standard coupled mode theory, which are obtained for both three-wave and four-wave mixing processes. Due to these reflections, the gain is enhanced and unwanted nonlinear phase modulations are suppressed. Predictions of the model are experimentally demonstrated on two types of unmatched TWPA, based on coplanar waveguides with a central wire consisting of (i) a high kinetic inductance superconductor, and (ii) an array of 2000 Josephson junctions.

DOI: 10.1103/PhysRevB.107.174520

I. INTRODUCTION

Modern microwave quantum engineering exploits efficient detection of low power microwave signals [1,2] requiring linear amplification with ultralow added noise. Nowadays, superconducting parametric amplifiers, exhibiting quantum limited sensitivity, have become the most favourable implementation in practical devices [3].

The superconducting parametric amplifiers that have been demonstrated so far can be divided in two classes: the resonant parametric amplifier [4–7] and the traveling wave parametric amplifier (TWPA) [8–11]. A resonant parametric amplifier works as a nonlinear resonator, which provides energy transfer from a strong pump tone to the signal to be amplified [12]. The finite interaction time of the waves providing amplification is enhanced by a high quality factor of the nonlinear resonator, which in turn limits the bandwidth. Typically, the required nonlinearity is achieved by integrating the resonator with an appropriate array of Josephson junctions (JJs) [13].

In a TWPA, the three-wave mixing (3WM) (in the presence of DC bias) or the four-wave mixing (4WM) process occurs, as waves propagate in a relatively long nonlinear transmission line (TL) [14]. The performance of the TWPA is usually described by coupled mode equations (CME) in the standard form for three types of waves: pump, signal, and idler, analogously to the fiber optics theory [15]. Standard CME predict that the bandwidth is limited by nonlinear phase modulations only. However, these modulations can be controlled by means of dispersion engineering. For instance, in Ref. [9], smoothed broadband amplification from 4 to 8 GHz has been achieved via 4WM and in Ref. [16] from 3.5 to 5.5 GHz under 3WM.

The analysis based on conventional CME, however, does not take into account counter-propagating waves reflected at the impedance mismatch between the nonlinear TL and standard 50 Ω circuitry. Despite the decade-long lasting effort, the development of an impedance matched device is still a challenge. In experiments, an impedance mismatch results in modulation of the amplifier transmission (ripples) [17,18]. This modulation can be significant, even more than 5 dB [8,9], which limits the applicability of these amplifiers. So far, these ripples have been described as Fabry-Pérot-like resonances [11,19] with the bandwidth inversely proportional to the length of the waveguide. Despite having significant influence on the amplifier transmission, the role of these resonances in parametric processes, to our best knowledge, has not been described satisfactorily.

Modifications of CME, required for photonic crystal engineering, account for reflections inside the photonic medium composing the TWPA [20–22]. In this paper, we generalize the conventional CME for both 3WM and 4WM processes, by taking into account the reflections at the ends of unmatched TWPA. This enables us to properly describe the transmission of broadband TWPAs, including resonance effects, such as gain enhancement analogous to the high quality resonant amplifiers. We have fabricated two coplanar waveguides, one made of high kinetic inductance (KI) superconductor, one consisting of 2000 JJs, both connected to 50 Ω input and output lines. They were tested in 3WM

*samuel.kern@fmph.uniba.sk

and 4WM regimes, respectively. A reasonable agreement between theory and experiment is demonstrated. Due to the impedance mismatch, both amplifiers operate in the intermediate regime between the resonant and the traveling-wave limits.

II. COUPLED MODE THEORY

Nonlinear media are commonly exploited for parametric amplification. In our case, such medium is provided by the middle wire of the TL, which is formed either by an array of JJs [see Fig. 4(b)] or by a high kinetic inductance superconductor. Dependencies of voltage $V(z,t)$ and current $I(z,t)$ on the coordinate (z) and time (t) in the TL are described by nonlinear telegrapher's equations:

$$\frac{\partial V(z,t)}{\partial t} = -\frac{1}{C_l}\frac{\partial I(z,t)}{\partial z}, \tag{1}$$

$$\frac{\partial I(z,t)}{\partial t} = -(L_l(1+I(z,t)^2/I_*^2))^{-1}\frac{\partial V(z,t)}{\partial z}, \tag{2}$$

where L_l and C_l denote the respective inductance and capacitance per unit length of the TL. Here I_* is scale of nonlinearity and relates to the critical current I_c, as will be discussed below. As the superconducting medium does not exhibit DC losses, the DC bias current I_D does not contribute to the voltage V, however, it alters the nonlinear inductance. Therefore, in the presence of I_D, Eq. (2) becomes

$$\frac{\partial I(z,t)}{\partial t} = -\left(L_l^D(1+\epsilon I(z,t)+\xi I(z,t)^2)\right)^{-1}\frac{\partial V(z,t)}{\partial z}, \tag{3}$$

where $\epsilon = 2I_D/(I_D^2+I_*^2)$, $\xi = 1/(I_D^2+I_*^2)$ [16] and the inductance per unit length enhanced by the DC bias is $L_l^D = L_l(1+I_D^2/I_*^2)$. In the following, $I(z,t)$ denotes only the RF current and I_D is fixed. Equivalently, Eqs. (1) and (3) can be presented as

$$v^2\frac{\partial^2 I(z,t)}{\partial z^2} - \frac{\partial^2 I(z,t)}{\partial t^2} = \frac{\partial^2}{\partial t^2}\left(\frac{1}{2}\epsilon I(z,t)^2 + \frac{1}{3}\xi I(z,t)^3\right), \tag{4}$$

where $v = 1/\sqrt{L_l^D C_l}$ is the phase velocity in the waveguide.

To extract the gain as a function of circuit parameters, typically four planar waves

$$I(z,t) = \sum_{\substack{n\in\\ \{p,s,i_3,i_4\}}} \frac{1}{2}(\mathcal{I}_n(z)e^{i(k_n z-\omega_n t)} + \text{c.c.}) \tag{5}$$

are substituted into Eq. (4). Here ω_n is the circular frequency and $k_n = \omega_n/v$ denotes the wave vector, where the index n indicates the type of the wave, namely, $n = p,\ s,\ i_3,\ i_4$ stands for pump, signal, and two idlers, respectively. The idler i_3 entering the 3WM satisfies

$$\omega_p = \omega_s + \omega_{i_3} \tag{6}$$

and 4WM idler i_4 obeys

$$2\omega_p = \omega_s + \omega_{i_4}. \tag{7}$$

Commonly, it is assumed that such waves propagate along an ideally matched TL. In practice, however, impedance mismatches at interconnections of different parts of the TL are present. This leads to partial reflection of the propagating waves, characterized by the reflection coefficient Γ_n determined by the impedance mismatch at the frequency ω_n. Taking such reflections at both ends of the nonlinear TL into account (see Appendix A), the RF current in the TL can be expressed as

$$I(z,t) = \sum_{\substack{n\in\\ \{p,s,i_3,i_4\}}} \frac{1}{2}(\mathcal{I}_n(z)t_n(e^{ik_n z}+\Gamma_n e^{-ik_n z})e^{-i\omega_n t} + \text{c.c.}), \tag{8}$$

where $t_n = 1/(1-\Gamma_n^2 e^{2ik_n l})$ is the transmission amplitude at the frequency ω_n and l is the length of the TL. Therefore the transmission coefficient can be expressed

$$T_n \equiv \left(1-\Gamma_n^2\right)^2|t_n|^2 = \frac{\left(1-\Gamma_n^2\right)^2}{1+\Gamma_n^4-2\Gamma_n^2\cos(2k_n l)}. \tag{9}$$

To reconstruct the functions $\mathcal{I}_s(z)$, $\mathcal{I}_{i_3}(z)$, and $\mathcal{I}_{i_4}(z)$, the expression (8) is substituted into the wave equation (4). Here, we emphasize that $\mathcal{I}_n(z)$ in the ansatz (8) can contain rapidly oscillating terms and, therefore, the amplitudes of the resulting forward and backward propagating modes of $I(z,t)$ could have a different spatial shape. However, utilizing the averaging method, we extract only a slowly varying part of the $\mathcal{I}_n(z)$ which mainly contributes to the forward propagation (see Appendixes A and B). From now on, we denote by symbol $\mathcal{I}_n(z)$ the slowly varying part of the aforementioned amplitudes only. Differential equations for the spatial evolution of these slowly varying amplitudes describing signal gain under 3WM and 4WM are obtained in an approximate form in the limit $\Gamma \ll 1$ (see Appendix B). Finally, a solution formally identical to the well-known equation for signal gain [15] is obtained from (B7):

$$\mathcal{G}_j(l) \equiv \left|\frac{\mathcal{I}_s(l)}{\mathcal{I}_s(0)}\right|^2 = \cosh^2(g_j l) + \frac{\beta_j^2}{4g_j^2}\sinh^2(g_j l), \tag{10}$$

where β_j is the parameter of the phase mismatch and g_j is the gain factor and index $j = 3$ or 4 indicates 3WM or 4WM, respectively. It is important to note that expression (10) is generalized to include reflections, which result in the following correction to the phase mismatch β_j and the gain factor g_j. The phase mismatch for 3WM process β_3 takes the form

$$\beta_3 = \Delta k_3\left(1+2\gamma\left(1+\Gamma_p^2\right)\right) - k_p\gamma\left(1-\Gamma_p^2\right), \tag{11}$$

where $\Delta k_3 = k_p - k_s - k_{i_3}$ is the mismatch of wave vectors and

$$\gamma = \frac{|t_p\mathcal{I}_p|^2}{8\left(I_D^2+I_*^2\right)} \tag{12}$$

is the strength of the nonlinearity. Now, the phase matching condition, i.e., $\beta_3 = 0$, dictates

$$\Delta k_3 = k_p\frac{\gamma\left(1-\Gamma_p^2\right)}{1+2\gamma\left(1+\Gamma_p^2\right)}. \tag{13}$$

Obviously, the presence of reflections suppresses the phase mismatch caused by the nonlinearity. Moreover, g_3 is increased, compared to a perfectly impedance-matched system

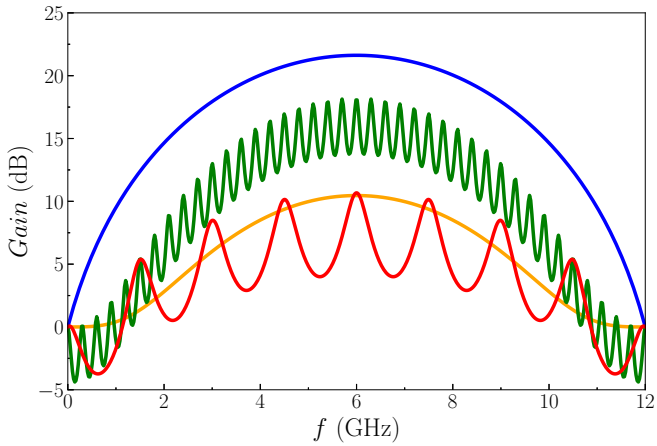

FIG. 1. Calculation of 4WM gain using standard CME ($\Gamma_p = 0$) for no dispersion engineering (orange curve) and for a perfect phase matching (blue curve). Parameters are taken from [11]. The green curve is prediction of modified theory [Eq. (17)] with $\Gamma_p = 0.45$ without any dispersion engineering. The red curve is the modified theory for 5 times shorter TL, no dispersion engineering and higher reflection coefficient $\Gamma_p = 0.6$. The gain of the short TL is comparable to standard theory prediction of long TL without phase-matching and the bandwith of each peak is ≈0.5 GHz.

with $\Gamma_p = 0$:

$$g_3 = \sqrt{k_s k_{i_3} \gamma \frac{8I_D^2}{\left(I_D^2 + I_*^2\right)}\left(1 + \Gamma_p^2\right) - \frac{\beta_3^2}{4}}. \tag{14}$$

The 4WM is obtained for zero DC bias, thus all waves participating in the mixing are partially reflected at the ends of the TWPA. This leads to even more radical changes. The phase mismatch β_4 is

$$\beta_4 = \Delta k_4\left(1 + 2\gamma\left(1 + \Gamma_p^2\right)\right) - 2k_p\gamma\left(1 - \Gamma_p^2\right), \tag{15}$$

where $\Delta k_4 = 2k_p - k_s - k_i$ is the mismatch of wave vectors under 4WM. The enhancement of the gain factor for 4WM is

$$g_4 = \sqrt{k_s k_{i_4} \gamma^2\left(1 + 4\Gamma_p^2\right) - \frac{\beta_4^2}{4}}. \tag{16}$$

Both current amplitudes—the amplified signal and the pump entering the γ coefficient [Eq. (12)]—are modulated by the Fabry-Pérot-like transmission amplitude t_n. Therefore the gain of the unmatched amplifier reads

$$G_j(l) \equiv \left|\frac{I_s(l)}{I_s(0)}\right|^2 = \mathcal{G}_j(l) T_s, \quad j = 3 \text{ and } 4. \tag{17}$$

To demonstrate the effect of reflections, we took the length and phase velocity from Ref. [11] and plotted the gain curves according to Eq. (17) in Fig. 1 for a demonstrative set of parameters. The resulting curves for the standard CME (or for $\Gamma_p = 0$) with and without phase matching are blue and orange, respectively. The green curve depicts the gain, according to Eq. (17), with $\Gamma = 0.45$ without phase matching. Sharp ripples appear and the gain is much higher in comparison to the orange curve. A 5 times shorter waveguide would result in much wider ripples and its gain (red curve) is comparable to the standard theory at original length.

According to Eqs. (10)–(17) the gain of a TWPA increases with the reflections occurring at the ends of the TL. Vice versa, as is shown in Appendix C, the presence of amplification changes the current and voltage wave propagation in such a way, that the reflections at the end of the TL are increased, too. This positive feedback may result in very high gain in the resonant peaks, whose quality is enhanced (ripples are sharpened). These so-called gain ripples are observed by many groups dealing with TWPA, even for nearly impedance-matched devices (aiming for $\Gamma_n \to 0$) [11,18]. The effect is not further studied here. In the presented experiment, this effect is observed as well and for measurements with a strong pump, a new value of Γ' is introduced.

III. EXPERIMENT

A. Kinetic inductance TWPA

In order to investigate the validity of the model described above, we fabricated the KI-TWPA device shown in Fig. 2. The design represents a waveguide where an inductive element—the central high-KI strip—is coupled to the ground plane via fractalized capacitors C_F (Fig. 2, bottom inset). The central strip is 27 mm long and 1 μm wide and has a sheet kinetic inductance of ∼4.2 pH/□. The combination of a highly inductive central strip and increased capacitance of fractalized capacitors results in slow propagation velocity (∼2% of the speed of light), thereby reducing the length of the transmission line required to get sufficient amplification [23,24]. Moreover, the width of the capacitors is periodically varied along the line to achieve dispersion engineering, with stop band at ≈10 GHz. In the vicinity of the band gap, the phase propagation velocity is perturbed, so that with a proper choice of the pump frequency the dispersion phase shift Δk_3 compensates for nonlinear phase shift acquired by high power pump and the $\beta = 0$ condition can be fulfilled [8].

The KI-TWPA chip was measured in a Helium gas-flow cryostat with a base temperature of ∼2 K. The input and output terminals of the device were bonded onto sampling lines in a printed circuit board (PCB) and the microwave transmission was measured using a vector network analyzer (VNA). In order to eliminate spurious ground plane resonances, the ground plane of the chip was carefully bonded to the PCB ground around the perimeter of the sample.

Figure 3 presents the amplifier's gain measured in 3WM operation regime for DC bias current $I_D = 1$ mA and the pump current amplitude $\mathcal{I}_p \approx 1$ mA at frequency 10.38 GHz. These values were precisely chosen to pump the amplifier at the edge of the band gap at the highest possible pump power, which does not break superconductivity. At optimal values, the phase-matching condition $\beta_3 = 0$ is fulfilled and high gain is achieved. The measured gain profile shows an average gain of 9.15 dB in the frequency range of 3–7 GHz, along with the presence of ripples indicating an impedance mismatch. As seen in Fig. 3 (inset), the ripples can be reasonably fitted with the proposed model. The reflection coefficient Γ_p and phase velocity v can be estimated from the fit, and are presented in Table I along with the values of $\mathcal{I}_p$ and I_D. For the kinetic inductance TWPA, I_* is derived within microscopic theory in Ref. [25] as $I_* \approx 2I_c$. However, in experiments, deviations

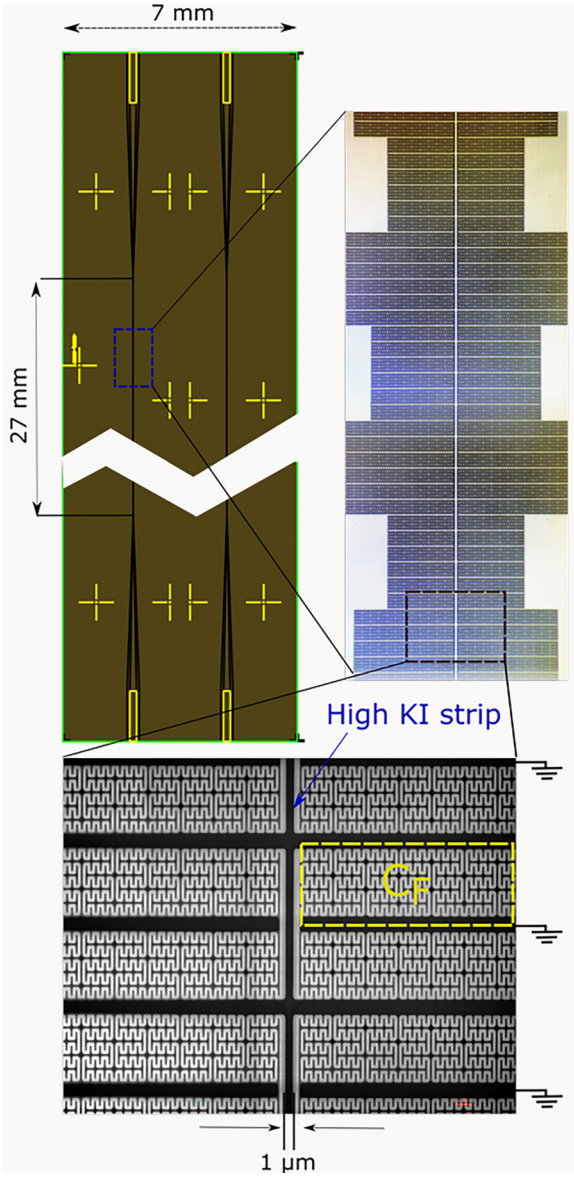

FIG. 2. Schematic of the KI-TWPA with chip dimensions. The right inset shows an optical micrograph of a few sections of quasi-fractal waveguide. The bottom inset is a magnified SEM image of the fractal structure. The width of the central high KI line is 1 μm.

from this value were observed. For example, in Ref. [26], for similar technology, the ratio I_*/I_c was estimated to be ≈5. This increase can be caused by the suppression of the critical current by vortex motion [27], and/or by the presence of weak spots in the middle wire. In other words, the average

TABLE I. Parameters of the KI-TWPA. The length l is given by the design, the other parameters are obtained from the fit of the amplification profile.

	l (mm)	$v[c]$	$I_D[I_*]$	$\mathcal{I}_p[I_*]$	Γ_p
standard theory	27	0.018	0.11	0.095	0
with correction			0.1	0.094	0.52

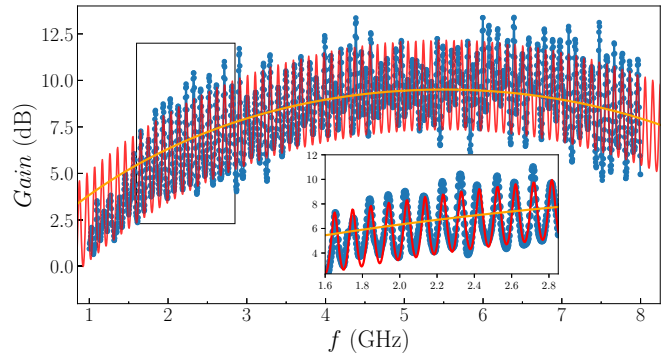

FIG. 3. Measured amplification of kinetic inductance TWPA (blue data). Red curve is a fit by the modified theory. The inset shows how the Fabry-Pérot oscillations were matched to the measured transmission, allowing the extraction of phase velocity and reflection coefficient utilized to reconstruct the frequency profile of the gain. The orange curve is a fit of the data by standard theory.

depairing current of the middle wire is higher than the critical current expected from the DC measurement. Therefore here we express the parameters $\mathcal{I}_p$ and I_D in units of I_*. A fit to the standard CM theory returns slightly higher values of I_D and $\mathcal{I}_p$ and lower amplification.

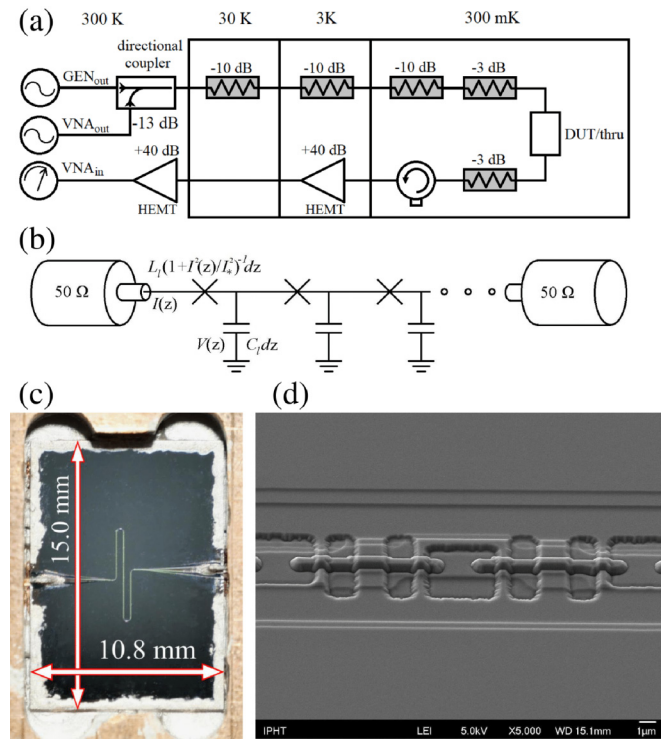

FIG. 4. (a) Transmission measurement setup in refrigerator. The 3 dB attenuator placed between the DUT and the isolator suppresses spurious resonances resulting from reflections between DUT and other parts of the setup. (b) Lumped element model of the JJ transmission line terminated by 50 Ω coaxial cables. Estimated values of inductance L_l and capacitance C_l are listed in Table II. (c) Photo of the TWPA chip in copper box connected to SMA connector by indium. The sample is grounded by conductive silver varnish. (d) SEM image of Nb/AlO/Nb JJs forming the middle wire of TWPA.

TABLE II. Parameters of the JJ-TWPA waveguide. The length l and the number of junctions N are set by design. NR_n is the room temperature resistance of the chain of N JJs. Other parameters are obtained from the fit of the weak signal transmission by Eq. (9) and the amplified signal transmission by the presumed model.

N	l (mm)	R_n (Ω)	I_c (μA)	L_l (pH/μm)	C_l (fF/μm)	$1/\sqrt{L_lC_l}[c]$	$\sqrt{L_l/C_l}$ (Ω)	Γ_s	Γ_s'	v [c]	$\mathcal{I}_p[I_c]$
2000	11	155	12.3	4.68	0.13	0.14	189	0.51	0.72	0.14	0.84

B. Josephson junction TWPA

To show that the effect of gain enhancement of a TWPA occurs even for a higher reflection coefficient ($\Gamma_p \approx 0.7$), a high impedance CPW with nonlinear inductance was studied (see Fig. 4). The middle wire, 11 mm long, is formed out of 2000 niobium-based Josephson junctions (JJs), see Appendix D as well as Ref. [28]. Assuming the inductance is dominated by the Josephson inductance, the inductance per unit length can be estimated by the relation $L_l l/2000 = \Phi_0/2\pi I_c$, where Φ_0 is the magnetic flux quantum. Here, the critical current I_c is estimated from the BCS relation for the product of I_c and the normal state resistance of the junction R_n [29]. The ground capacitance is estimated both by the standard formula (see Ref. [30]), and an EM simulation in SONNET software. These values, listed in Table II, are utilized in the estimation of the phase velocity $1/\sqrt{L_lC_l}$ and the characteristic impedance $\sqrt{L_l/C_l}$. The design also contains photonic-crystal-like impedance modulation, however at the actual length of the waveguide, it has no observable effect.

The sample was installed in a copper box and its 50 Ω contacting pads were connected to the SMA connectors by indium [see Fig. 4(c)]. Prior to the actual measurement, the transmission has been calibrated by using a 50 Ω TL connected instead of the TWPA (for details on calibration, see Ref. [31]) by a VNA in a pulse-tube refrigerator at a temperature of 3.5 K according to scheme shown in Fig. 4(a).

Transmission measurement of the unmatched TL was performed at low signal power, where nonlinearity is negligible (see blue line in Fig. 5). The measured transmission exhibits resonances, with peaks at frequencies $f_m = mv/2l$, where m is an integer and l is the length of the waveguide. As the unmatched waveguide creates a stepped impedance resonator, the transmission can be described by Eq. (9) plotted as red line in Fig. 5.

The obtained phase velocity v and the reflection coefficient Γ_s of the waveguide are consistent with the estimated inductance and capacitance per unit length (see Table II). These parameters are used to calculate the gain of the TWPA from Eq. (17). In addition, the reflection coefficient Γ_s is increased after the pump is applied and amplification is observed (see Appendix C). Therefore Γ_s was replaced by the value $\Gamma_s' \approx 0.72$ obtained as a best fit to the experimental blue line by the theoretical red curve in Fig. 6.

The signal transmission with pump tone on was measured for various signal and pump powers. The highest amplification was achieved for pump power of −57.0 dBm and signal power ranging from −100 to −86 dBm at the input of the device. Figure 6 presents the gain as a function of the signal frequency, at the pump frequency of 3.38 GHz. As there were no dispersion engineering features, and $\Delta k_4 = 0$ holds for all pump frequencies, a similar gain profile was obtained at various pump frequencies. The measured gain profile shows a region where the amplification occurs, clearly corresponding to a peak resulting from resonance caused by the impedance mismatch (Fig. 5). When the standard model for matched TL is applied ($\Gamma_p = 0$, see orange curve in Fig. 6), a weak amplification (< 5 dB) is obtained over a wide bandwidth. Including the effects of reflections by the discussed model and accounting for the correction $\Gamma_p = \Gamma_s'$ from Table II improves the correspondence between the theory and experiment. The ratio between the nonlinearity scale and the critical current for JJs is more robust and it is given as $I_*/I_c = \sqrt{2}$. As the critical current estimated from the Josephson inductance agrees with the value calculated from the resistance of junctions, the pump current amplitude is expressed in units of I_c.

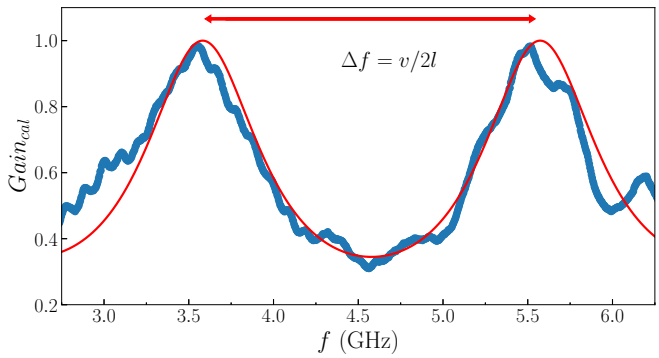

FIG. 5. (a) Calibrated weak signal transmission without pumping tone (blue line). Fit of the data by Fabry-Pérot oscillating transmission (9) (red curve). The parameters of the fit; Γ_s and v, are listed in Table II.

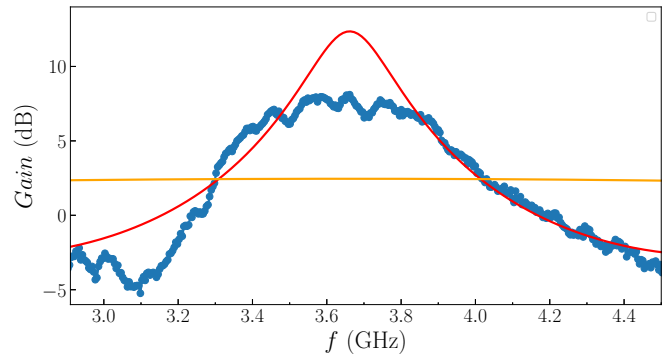

FIG. 6. The measured gain of the TWPA (blue line) for the pump frequency of 3.38 GHz. Orange and red curves are the results of the standard CME and the model with reflections for $\Gamma_p = 0.72$, respectively.

IV. CONCLUSION

In this paper, we presented a modification of standard CME for parametric amplification, which is commonly utilized to analyze TWPAs. By considering reflections due to impedance mismatches, we showed that the gain ripples are an inherent property of unmatched finite length TWPAs. Similarly to resonant amplifiers, in these peaks, the presented theory predicts enhanced gain. This feature can be utilized in the design of shorter TWPAs. A shorter TL results in the broadening of gain ripples with bandwidth from few MHz up to 1 GHz and, at the same time, providing reasonable gain. The operating frequency range, where the unmatched TWPA provides gain in a series of Fabry-Pérot-like resonances is also increased by the reflections. Therefore these peaks could be utilized in experiments requiring multiplexing.

Less demanding fabrication of the shorter TWPAs and omitting the challenging impedance matching may be advantages. In this paper, therefore, we studied the working regime of TWPA, in which the gain is increased by the reflections and the bandwidth is given by Fabry-Pérot resonances. We demonstrate the usability of our model by analyzing the response of two types of devices: a JJ and a kinetic inductance TWPA. For the kinetic inductance TWPA 27 mm long with slight impedance mismatch, good agreement with the experiment was achieved. Series of 30–40 MHz wide peaks with gain over 10 dB are observed in range from 3–7 GHz. The JJ TPWA was significantly shorter ($l = 11$ mm) with higher reflections providing 8 dB gain in a single peak with the bandwidth of ≈600 MHz.

ACKNOWLEDGMENTS

We thank L. Planat and N. Roch (Institut Néel, CNRS, Grenoble) and D. M. Basko (Université Grenoble Alpes, CNRS, LPMMC, Grenoble) for useful discussions. This work was supported by the European Unions Horizon 2020 research and innovation programme under Grant Agreement No. 863313 (SUPERGALAX), No. 362660 (Quantum E-Leaps), and by the SAS-MVTS, Grant QuantERA-SiUCs. The support from the Slovak Research and Development Agency under the Contracts No. APVV-16-0372, No. APVV-20-0425 are gratefully acknowledged. The Chalmers group acknowledges the support from the Swedish Research Council (VR) (Grant Agreements No. 2016-04828 and No. 2019-05480), EU H2020 European Microkelvin Platform (Grant Agreement No. 824109), Engineering and Physical Sciences Research Council (EPSRC) Grant No. EP/T004088/1 and from Knut and Alice Wallenberg Foundation via the Wallenberg center for Quantum Technology (WACQT). This work has relieved funding from German Federal Ministry of Education and Research (BMBF) under the project QSolid (Grant No. 13N16152) and the Free State of Thuringia under No. 2021 FGI 0049.

APPENDIX A: COUPLED MODE EQUATIONS FOR WAVES IN A RESONATOR

The field inside a Fabry-Pérot resonator terminated by two identical mirrors with reflection coefficients Γ_n consists of an infinite number of reflected waves. Thus the amplitude I_n of the field oscillating at frequency ω_n is defined as

$$\begin{aligned} &I_n(z,t) \\ &= \tfrac{1}{2}\mathcal{I}_n(z)(e^{ik_n z} + \Gamma_n e^{ik_n(l-z)} + \Gamma_n^2 e^{ik_n(2l+z)} + \ldots)e^{-i\omega_n t} + \text{c.c.} \\ &= \tfrac{1}{2}\mathcal{I}_n(z)t_n(e^{ik_n z} + \tilde{\Gamma}_n e^{-ik_n z})e^{-i\omega_n t} + \text{c.c.}, \end{aligned} \tag{A1}$$

where in the last line, the following notation is introduced

$$\tilde{\Gamma}_n = \Gamma_n e^{ik_n l}, \tag{A2}$$

$$t_n = \frac{1}{1-\tilde{\Gamma}_n^2}. \tag{A3}$$

Solving the nonlinear wave equation (4) for current in the form $I(z,t) = I_s(z,t) + I_p(z,t) + I_{i_3}(z,t) + I_{i_4}(z,t)$ means finding the spatially dependent current amplitudes $\mathcal{I}_n(z)$, such that the current (8), satisfies (4). Substituting (8) into (4) and adopting notation $\mathcal{I}_n' \equiv \frac{\partial \mathcal{I}_n}{\partial z}$, one obtains within a slowly varying envelope approximation (i.e., $|\mathcal{I}_n''| \ll k_n|\mathcal{I}_n'|$) the following equation:

$$\begin{aligned} &\frac{1}{L_l C_l} ik_n \mathcal{I}_n'(z) t_n(e^{ik_n z} - \tilde{\Gamma}_n e^{-ik_n z}) = \\ &\quad - \frac{\epsilon\omega_n^2}{2} \sum_{\substack{a,b\in \\ \{p,s,i_3\}}} \left(\prod_{\substack{m\in \\ \{a,b\}}} \frac{1}{2}\mathcal{I}_m^{\pm} t_m^{\pm}(e^{\pm ik_m z} + \tilde{\Gamma}_m^{\pm} e^{\mp ik_m z}) \right) \\ &\quad \times \delta(\omega_n \mp \omega_a \mp \omega_b) \\ &\quad - \frac{\xi\omega_n^2}{3} \sum_{\substack{a,b,c\in \\ \{p,s,i_4\}}} \left(\prod_{\substack{m\in \\ \{a,b,c\}}} \frac{1}{2}\mathcal{I}_m^{\pm} t_m^{\pm}(e^{\pm ik_m z} + \tilde{\Gamma}_m^{\pm} e^{\mp ik_m z}) \right) \\ &\quad \times \delta(\omega_n \mp \omega_a \mp \omega_b \mp \omega_c), \end{aligned} \tag{A4}$$

where the first sum on the right-hand side describes 3WM terms and the second includes 4WM terms. Here, $\mathcal{I}_m^+ = \mathcal{I}_m$, $t_m^+ = t_m$ and $\tilde{\Gamma}_m^+ = \tilde{\Gamma}_m$, whereas $\mathcal{I}_m^- = \mathcal{I}_m^*$, $t_m^- = t_m^*$ and $\tilde{\Gamma}_m^- = \tilde{\Gamma}_m^*$, i.e., minus in superscript indicates complex conjugation.

To study the parametric amplification provided by three- and four-wave mixing Eq. (A4) is solved for four waves: strong pump $\mathcal{I}_p$, signal $\mathcal{I}_s$ and two idlers $\mathcal{I}_{i_{3,4}}$ such that $\mathcal{I}_p \gg \mathcal{I}_s, \mathcal{I}_{i_{3,4}}$. Making use of conditions (6) and (7) in the delta functions in equation (A4), one obtains

$$\mathcal{I}_p' = \frac{ik_p}{8}\xi|\mathcal{I}_p|^2|t_p|^2\mathcal{I}_p\mathcal{F}_{pp}^{pp}, \tag{A5}$$

$$\begin{aligned} \mathcal{I}_s' = &\frac{ik_s}{4}\epsilon\mathcal{I}_p\mathcal{I}_{i_3}^* \frac{t_p t_{i_3}^*}{t_s}\mathcal{F}_{i_3 s}^{p} \\ &+ \frac{ik_s}{8}\xi\left(\mathcal{I}_p^2\mathcal{I}_{i_4}^* \frac{t_p^2 t_{i_4}^*}{t_s}\mathcal{F}_{i_4 s}^{pp} + 2|\mathcal{I}_p|^2\mathcal{I}_s|t_p|^2\mathcal{F}_{ps}^{ps}\right), \end{aligned} \tag{A6}$$

$$\mathcal{I}_{i_3}' = \frac{ik_{i_3}}{4}\left(\epsilon\mathcal{I}_p\mathcal{I}_s^* \frac{t_p t_s^*}{t_{i_3}}\mathcal{F}_{si_3}^{p} + \xi|\mathcal{I}_p|^2\mathcal{I}_{i_3}|t_p|^2\mathcal{F}_{pi_3}^{pi_3}\right), \tag{A7}$$

$$\mathcal{I}_{i_4}' = \frac{ik_{i_4}}{8}\xi\left(\mathcal{I}_p^2\mathcal{I}_s^* \frac{t_p^2 t_s^*}{t_{i_4}}\mathcal{F}_{si_4}^{pp} + 2|\mathcal{I}_p|^2\mathcal{I}_{i_4}|t_p|^2\mathcal{F}_{pi_4}^{pi_4}\right), \tag{A8}$$

where

$$\mathcal{F}^{ab}_{cd}(z) = (e^{ik_a z} + \tilde{\Gamma}_a e^{-ik_a z})(e^{ik_b z} + \tilde{\Gamma}_b e^{-ik_b z}) \times \frac{(e^{-ik_c z} + \tilde{\Gamma}^*_c e^{ik_c z})}{e^{ik_d z} - \tilde{\Gamma}_d e^{-ik_d z}}, \quad a, b, c, d \in \{p, s, i_3, i_4\}, \tag{A9}$$

$$\mathcal{F}^{a}_{cd}(z) = (e^{ik_a z} + \tilde{\Gamma}_a e^{-ik_a z}) \frac{(e^{-ik_b z} + \tilde{\Gamma}^*_b e^{ik_b z})}{e^{ik_c z} - \tilde{\Gamma}_c e^{-ik_c z}}, \times\ a, b, c \in \{p, s, i_3\}. \tag{A10}$$

The equation for pump (A5) is solved in the depleted pump approximation $|\mathcal{I}_p|' = 0$:

$$\mathcal{I}_p = |\mathcal{I}_p| \exp\left(i \int_0^z \tilde{\tilde{\kappa}}_p \mathcal{F}^{pp}_{pp} dx \right), \tag{A11}$$

where

$$\tilde{\tilde{\kappa}}_n = k_n \frac{|\mathcal{I}_p|^2 t_p^2}{8} \xi = k_n \frac{|\mathcal{I}_p|^2 t_p^2}{8} \frac{1}{(I_D^2 + I_*^2)}, \tag{A12}$$

$$\tilde{\tilde{\kappa}}_n = k_n \frac{t_p \mathcal{I}_p}{4} \epsilon = k_n \frac{t_p \mathcal{I}_p}{4} \frac{2 I_D}{(I_D^2 + I_*^2)}. \tag{A13}$$

Although the exponential in Eq. (A11) contains also a real part, changing the module $|\mathcal{I}_p|$ too, the contribution oscillates at the scale of $1/k_p$ and it is smaller than imaginary part by factor Γ_p, thus it is neglected. Utilizing solution (A11), Eqs. (A6)–(A8) are simplified by the following transformation:

$$A_n = \mathcal{I}_n t_n \exp\left(-2i \int_0^z \tilde{\tilde{\kappa}}_n \mathcal{F}^{pn}_{pn} dx \right), \quad n = s,\ i_3,\ \text{and}\ i_4. \tag{A14}$$

Finally, one obtains the coupled mode equations for the complex amplitudes A_s and $A_{i_{3,4}}$:

$$A'_s = i\tilde{\tilde{\kappa}}_s A^*_{i_3} \mathcal{F}^{p}_{i_3 s} e^{ib_3} + i\tilde{\tilde{\kappa}}_s A^*_{i_4} \mathcal{F}^{pp}_{i_4 s} e^{ib_4}, \tag{A15}$$

$$A'_{i_3} = i\tilde{\tilde{\kappa}}_{i_3} A^*_s \mathcal{F}^{p}_{s i_3} e^{ib_3}, \tag{A16}$$

$$A'_{i_4} = i\tilde{\tilde{\kappa}}_{i_4} A^*_s \mathcal{F}^{pp}_{s i_4} e^{ib_4}. \tag{A17}$$

Here, the functions $b_3(z)$ and $b_4(z)$ contain contributions to the nonlinear phase modulations and are expressed as follows:

$$b_3(z) = \int_0^z \left(\tilde{\tilde{\kappa}}_p \mathcal{F}^{pp}_{pp}(x) - 2\tilde{\tilde{\kappa}}_s \mathcal{F}^{ps}_{ps}(x) - 2\tilde{\tilde{\kappa}}_{i_3} \mathcal{F}^{p i_3}_{p i_3}(x) \right) dx, \tag{A18}$$

$$b_4(z) = 2 \int_0^z \left(\tilde{\tilde{\kappa}}_p \mathcal{F}^{pp}_{pp}(x) - \tilde{\tilde{\kappa}}_s \mathcal{F}^{ps}_{ps}(x) - \tilde{\tilde{\kappa}}_{i_4} \mathcal{F}^{p i_4}_{p i_4}(x) \right) dx. \tag{A19}$$

In the following sections, the obtained equations are solved in two cases: (1) $I_D \gg \mathcal{I}_p$ (three-wave mixing) [16,22] and (2) $I_D = 0$ (four-wave mixing).

1. Three-wave mixing

To study 3WM, let us assume that the DC bias current is much larger than the pump amplitude, which means, according to Eqs. (A12) and (A13), that $\tilde{\tilde{\kappa}}_n \gg \tilde{\tilde{\kappa}}_n$. If no idler is applied at the frequency ω_{i_4} to the input of the device, the 4WM idler is generated proportionally to $\tilde{\tilde{\kappa}}_{i_4}$. Therefore the 4WM idler is much weaker than 3WM idler which is proportional to $\tilde{\tilde{\kappa}}_{i_3}$ and the system of equations (A15)–(A17) is approximated by two coupled equations

$$A'_s = i\tilde{\tilde{\kappa}}_s A^*_{i_3} \mathcal{F}^{p}_{i_3 s} e^{ib_3}, \tag{A20}$$

$$A'_{i_3} = i\tilde{\tilde{\kappa}}_{i_3} A^*_s \mathcal{F}^{p}_{s i_3} e^{ib_3}, \tag{A21}$$

which can be easily decoupled. For A_s, the uncoupled equation is

$$A''_s - \frac{\left(e^{ib_3} \mathcal{F}^{p}_{i_3 s}\right)'}{e^{ib_3} \mathcal{F}^{p}_{i_3 s}} A'_s - \tilde{\tilde{\kappa}}_s \mathcal{F}^{p}_{i_3 s} \left(\tilde{\tilde{\kappa}}_{i_3} \mathcal{F}^{p}_{s i_3}\right)^* A_s e^{-i2\Im\mathfrak{m}(b_3)} = 0. \tag{A22}$$

2. Four-wave mixing

When no DC bias is applied, pure 4WM is observed and the system (A15)–(A17) becomes

$$A'_s = i\tilde{\tilde{\kappa}}_s A^*_{i_4} \mathcal{F}^{pp}_{i_4 s} e^{ib_4}, \tag{A23}$$

$$A'_{i_4} = i\tilde{\tilde{\kappa}}_{i_4} A^*_s \mathcal{F}^{pp}_{s i_4} e^{ib_4}, \tag{A24}$$

which gives the equation for the spatial evolution of the transformed signal amplitude $A_s(z)$:

$$A''_s - \frac{\left(e^{ib_4} \mathcal{F}^{pp}_{i_4 s}\right)'}{e^{ib_4} \mathcal{F}^{pp}_{i_4 s}} A'_s - \tilde{\tilde{\kappa}}_s \mathcal{F}^{pp}_{i_4 s} \left(\tilde{\tilde{\kappa}}_{i_4} \mathcal{F}^{pp}_{s i_4}\right)^* A_s e^{-i2\Im\mathfrak{m}(b_4)} = 0, \tag{A25}$$

A simple check of our derivation is achieved by identifying Eqs. (A22) and (A25) as the general form of the standardly presented CME result for $\Gamma_n = 0$.

APPENDIX B: APPROXIMATION OF THE GAIN EQUATION

Equations (A22) and (A25) for slow variation of an envelope of waves propagating and reflecting in a nonlinear Fabry-Pérot resonator are second-order differential equations where $\mathcal{F}$ and b are functions of z. To solve the differential equations, we expand these functions up to second order in the reflection coefficient $\Gamma_n < 1$ and remove terms with harmonic spatial dependence via the averaging method [32]. This transformation is indicated by the arrows in the equations given below. This procedure yields an equation similar to the result of the standard CME for waves propagating only in one direction:

$$\mathcal{F}^{pp}_{pp} \approx 1 + 2\Gamma_p e^{-ik_p(2z-l)} + 2\Re\mathfrak{e}(\Gamma_p e^{-ik_p(2z-l)}) + 3|\Gamma_p|^2 + 4\Gamma_p^2 e^{-i2k_p(2z-l)} \to 1 + 3|\Gamma_p|^2, \tag{B1}$$

$$\mathcal{F}^{pn}_{pn} \approx 1 + 2\Gamma_n e^{-ik_n(2z-l)} + 2\Gamma_n^2 e^{-ik_s(2z-l)} + 2\Re\mathfrak{e}(\Gamma_p e^{-ik_p(2z-l)})(1 + 2\Gamma_n e^{-i(k_n)(2z-l)}) + |\Gamma_p|^2 \to 1 + |\Gamma_p|^2, \quad n = s,\ i_4, \tag{B2}$$

$$\mathcal{F}^{p\ *}_{s i_3} \mathcal{F}^{p}_{i_3 s} \to 1 + |\Gamma_p|^2, \tag{B3}$$

$$\mathcal{F}^{pp*}_{s i_4} \mathcal{F}^{pp}_{i_4 s} \to 1 + 4|\Gamma_p|^2. \tag{B4}$$

The above approximations leads to the equation describing 3WM

$$A_s'' - i\beta_3 A_s' - \tilde{\tilde{\kappa}}_s \tilde{\tilde{\kappa}}_{i_3}^* (1 + |\Gamma_p|^2) A_s = 0, \tag{B5}$$

which gives the nonlinear phase mismatch β_3

$$\beta_3 = \Delta k_3 + \tilde{\tilde{\kappa}}_p (1 + 3|\Gamma_p|^2) - 2\tilde{\tilde{\kappa}}_s (1 + |\Gamma_p|^2) - 2\tilde{\tilde{\kappa}}_{i_3} (1 + |\Gamma_p|^2)), \tag{B6}$$

where $\Delta k_3 = k_p - k_s - k_{i_3}$ is the deviation from linear dispersion relation.

Similarly, the differential equation for 4WM takes the form

$$A_s'' - i\beta_4 A_s' - \tilde{\tilde{\kappa}}_s \tilde{\tilde{\kappa}}_{i_4}^* (1 + 4|\Gamma_p|^2) A_s = 0 \tag{B7}$$

and the nonlinear phase mismatch β_4 reads

$$\beta_4 = \Delta k_4 + 2(\tilde{\tilde{\kappa}}_p (1 + 3|\Gamma_p|^2) - \tilde{\tilde{\kappa}}_s (1 + |\Gamma_p|^2) - \tilde{\tilde{\kappa}}_{i_4} (1 + |\Gamma_p|^2)), \tag{B8}$$

where $\Delta k_4 = 2k_p - k_s - k_{i_4}$.

With the boundary conditions $\mathcal{I}_s(z=0) = \mathcal{I}_{s0}$ and $\mathcal{I}_{i_{3,4}}(z=0) = 0$, the solution takes the compact form

$$\mathcal{I}_s(z) = \mathcal{I}_{s0} \left(\cosh(g_{3,4} z) - i \frac{\beta_{3,4}}{2 g_{3,4}} \sinh(g_{3,4} z) \right) \times e^{i\left(\frac{\beta_{3,4}}{2} + 2\tilde{\tilde{\kappa}}_s (1 + |\Gamma_p|^2)\right) z}, \tag{B9}$$

where

$$g_3 = \sqrt{\tilde{\tilde{\kappa}}_s \tilde{\tilde{\kappa}}_{i_3}^* (1 + |\Gamma_p|^2) - \frac{\beta_3^2}{4}}, \tag{B10}$$

$$g_4 = \sqrt{\tilde{\tilde{\kappa}}_s \tilde{\tilde{\kappa}}_{i_4}^* (1 + 4|\Gamma_p|^2) - \frac{\beta_4^2}{4}} \tag{B11}$$

are gain factors for 3WM and 4WM, respectively.

APPENDIX C: QUALITY INCREASE DUE TO AMPLIFICATION

Following the conventional derivation of the reflection coefficient Γ_n at the ends of the TL (see Ref. [33]), we derive below the influence of the amplification on the reflection coefficient and, therefore, on the quality factor of the resonator. Utilizing the first telegrapher equation (1) for harmonic components:

$$I_n'(z) = -i\omega_s C V_n(z), \tag{C1}$$

the voltage amplitude along the waveguide is found by substituting the current amplitude, which was determined in the previous Appendix (Appendix A). This way the impedance at the end of the waveguide is obtained:

$$Z_n(l) = \frac{V_s(l)}{I_s(l)} \approx Z_0 \left(1 + i \frac{\mathcal{I}_n(z)'|_{z=l}}{\mathcal{I}_n(l) k_n}\right), \tag{C2}$$

where $Z_0 = \sqrt{L_l / C_l}$ and the nonlinear spatial variation of phase velocity was neglected. Finally, the reflection coefficient can by expressed as

$$\Gamma_n = \frac{Z_L - Z_0 - Z_0 i \frac{\mathcal{I}_n(z)'|_{z=l}}{\mathcal{I}_n(l) k_n}}{Z_L + Z_0 + Z_0 i \frac{\mathcal{I}_n(z)'|_{z=l}}{\mathcal{I}_n(l) k_n}}, \tag{C3}$$

showing that the reflection is sensitive to any spatial variation in the amplitude of the current.

APPENDIX D: SAMPLES PREPARATION

The 140 nm NbN film for a KI-TWPA was fabricated at Chalmers, following the recipe Ref. [26]. These films were deposited on a sapphire wafer and the desired structure was patterned with e-beam lithography and Ar:Cl_2 plasma etching. The central line was further thinned down to 30 nm, to get a sheet resistance of ∼48 Ω/□, which corresponds to the desired kinetic inductance of ∼4 pH/□. The thickness of the ground plane and other elements was left unchanged, in order to keep the KI of these elements low and thereby eliminate self-resonances in fractal structures.

The JJ devices were fabricated at Leibniz IPHT by making use of the so-called cross-type Josephson junction technology. Here a trilayer of Nb/AlO_x/Nb with a critical current density of about 1.7 kA/cm^2 is deposited on an oxidized 4 inch silicon wafer of 500 μm thickness. Thermal oxide thickness on the wafer was about 600 nm. Inside a meander shaped Nb groundplane with a 9 μm slit, an array of Josephson junctions form the center conductor. In total, 2000 Josephson junctions with a nominal junction size of (0.9 × 0.9) μm^2 are fabricated on a single chip, with dimensions of (10800 × 15000) μm^2. By means of Fiske step measurements, the specific junction capacitance has been determined to be around 60 fF/μm^2 for this critical current density. For sample fabrication, electron beam lithography has been used. Nb patterning was done by making use of reactive ion etching based on CF_4.

[1] P. Krantz, M. Kjaergaard, F. Yan, T. P. Orlando, S. Gustavsson, and W. D. Oliver, Appl. Phys. Rev. **6**, 021318 (2019).

[2] E. Il'ichev, A. Smirnov, M. Grajcar, A. Izmalkov, D. Born, N. Oukhanski, T. Wagner, W. Krech, H.-G. Meyer, and A. Zagoskin, Low Temp. Phys. **30**, 620 (2004).

[3] M. Devore and R. Ananda, C. R. Phys. **17**, 740 (2016).

[4] B. Yurke, J. Opt. Soc. Am. B **4**, 1551 (1987).

[5] B. Yurke, L. R. Corruccini, P. G. Kaminsky, L. W. Rupp, A. D. Smith, A. H. Silver, R. W. Simon, and E. A. Whittaker, Phys. Rev. A **39**, 2519 (1989).

[6] B. Yurke, M. Roukes, R. Movshovich, and A. Pargellis, Appl. Phys. Lett. **69**, 3078 (1996).

[7] A. M. Zagoskin, E. Il'ichev, M. W. McCutcheon, J. F. Young, and F. Nori, Phys. Rev. Lett. **101**, 253602 (2008).

[8] B. H. Eom, P. K. Day, H. G. LeDuc, and J. Zmuidzinas, Nat. Phys. **8**, 623 (2012).
[9] T. White, J. Mutus, I.-C. Hoi, R. Barends, B. Campbell, Y. Chen, Z. Chen, B. Chiaro, A. Dunsworth, E. Jeffrey *et al.*, Appl. Phys. Lett. **106**, 242601 (2015).
[10] C. Macklin, K. O'brien, D. Hover, M. Schwartz, V. Bolkhovsky, X. Zhang, W. Oliver, and I. Siddiqi, Science **350**, 307 (2015).
[11] L. Planat, A. Ranadive, R. Dassonneville, Puertas Martínez, J., S. Léger, C. Naud, O. Buisson, W. Hasch-Guichard, D. M. Basko, and N. Roch, Phys. Rev. X **10**, 021021 (2020).
[12] E. A. Tholén, A. Ergül, E. M. Doherty, F. M. Weber, F. Grégis, and D. B. Haviland, Appl. Phys. Lett. **90**, 253509 (2007).
[13] M. Castellanos-Beltran and K. Lehnert, Appl. Phys. Lett. **91**, 083509 (2007).
[14] M. R. Vissers, R. P. Erickson, H.-S. Ku, L. Vale, X. Wu, G. Hilton, and D. P. Pappas, Appl. Phys. Lett. **108**, 012601 (2016).
[15] G. P. Agrawal, *Nonlinear Fiber Optics*, 3rd ed. (Academic Press, 2001).
[16] M. Malnou, M. R. Vissers, J. D. Wheeler, J. Aumentado, J. Hubmayr, J. N. Ullom, and J. Gao, PRX Quantum **2**, 010302 (2021).
[17] S. Chaudhuri, D. Li, K. Irwin, C. Bockstiegel, J. Hubmayr, J. Ullom, M. Vissers, and J. Gao, Appl. Phys. Lett. **110**, 152601 (2017).
[18] S. Goldstein, N. Kirsh, E. Svetitsky, Y. Zamir, O. Hachmo, C. E. M. de Oliveira, and N. Katz, Appl. Phys. Lett. **116**, 152602 (2020).
[19] S. Zhao and S. Withington, J. Phys. D **54**, 365303 (2021).
[20] W.-P. Huang, J. Opt. Soc. Am. A **11**, 963 (1994).
[21] T. Christopoulos, O. Tsilipakos, G. Sinatkas, and E. E. Kriezis, Phys. Rev. B **98**, 235421 (2018).
[22] R. P. Erickson and D. P. Pappas, Phys. Rev. B **95**, 104506 (2017).
[23] S. d. Graaf, A. Danilov, A. Adamyan, T. Bauch, and S. Kubatkin, J. Appl. Phys. **112**, 123905 (2012).
[24] A. Adamyan, S. De Graaf, S. Kubatkin, and A. Danilov, J. Appl. Phys. **119**, 083901 (2016).
[25] A. V. Semenov, I. A. Devyatov, M. P. Westig, and T. M. Klapwijk, Phys. Rev. Appl. **13**, 024079 (2020).
[26] S. Mahashabde, E. Otto, D. Montemurro, S. de Graaf, S. Kubatkin, and A. Danilov, Phys. Rev. Appl. **14**, 044040 (2020).
[27] A. Engel, H. Bartolf, A. Schilling, K. Il'in, M. Siegel, A. Semenov, and H. Hübers, J. Phys.: Conf. Ser. **97**, 012152 (IOP, 2008).
[28] S. Anders, M. Schmelz, L. Fritzsch, R. Stolz, V. Zakosarenko, T. Schönau, and H. Meyer, Supercond. Sci. Technol. **22**, 064012 (2009).
[29] V. Ambegaokar and A. Baratoff, Phys. Rev. Lett. **10**, 486 (1963).
[30] M. Göppl, A. Fragner, M. Baur, R. Bianchetti, S. Filipp, J. M. Fink, P. J. Leek, G. Puebla, L. Steffen, and A. Wallraff, J. Appl. Phys. **104**, 113904 (2008).
[31] S. Kern, P. Neilinger, D. Manca, E. Il'ichev, M. Schmelz, J. Kunert, G. Oelsner, R. Stolz, and M. Grajcar, *Proceedings of the 32th International Conference on Applied Physics of Condensed Matter* (FEI STU, Bratislava, 2021).
[32] J. A. Sanders, F. Verhulst, and J. Murdock, *Averaging Methods in Nonlinear Dynamical Systems* (Springer, 2007), Vol. 59.
[33] D. M. Pozar, *Microwave Engineering* (Wiley, 2011).